Reports of Practical Oncology and Radiotherapy 25 (2020) 961–968

Available online at www.sciencedirect.com

Reports of Practical Oncology and Radiotherapy

journal homepage: http://www.elsevier.com/locate/rpor

Original research article

Normal lung tissue complication probability in MR-Linac and conventional radiotherapy

Somayeh Gholami[a,b,*], Francesco Longo[c], Sara Shahzadeh[d], Hassan Ali Nedaie[a,b], Ryan Sharp[e], Ali S.Meigooni[f]

[a] Radiation Oncology Research Centre, Cancer Institute, Tehran University of Medical Sciences, Tehran, Iran
[b] Department of Medical Physics and Biomedical Engineering, Tehran University of Medical Sciences, Tehran, Iran
[c] Department of Physics, University of Trieste and INFN Trieste, Italy
[d] Department of Medical Radiation Engineering, Shahid Beheshti University, Tehran, Iran
[e] Department of Health Physics and Diagnostic Sciences, University of Nevada, Las Vegas, Nevada, United States
[f] Comprehensive Cancer Centers of Nevada, Las Vegas, Nevada, United States

ARTICLE INFO

Article history:
Received 3 June 2020
Accepted 10 September 2020
Available online 29 September 2020

Keywords:
Normal lung tissue complications
MR-linac
Geant4 toolkit
XCAT digital phantom

ABSTRACT

Purpose: To study normal lung tissue (NLT) complications in magnetic resonance (MR) image based linac and conventional radiotherapy (RT) techniques.
Materials and Methods: The Geant4 toolkit was used to simulate a 6 MV photon beam. A homogenous magnetic field of 1.5 Tesla (T) was applied in both perpendicular and parallel directions relative to the radiation beam.

Analysis of the NLT complications was assessed according to the normal lung tissue complication probability (NTCP), the mean lung dose (MLD), and percentage of the lung volume receiving doses greater than 20 Gy (V_{20}), using a sample set of CT images generated from a commercially available 4D-XCAT digital phantom.
Results: The results show that the MLD and V_{20} were lower for MR-linac RT. The largest reduction of MLD and V_{20} for MR-linac RT configurations were 5 Gy and 29.3%, respectively.
Conclusion: MR-linac RT may result in lower NLT complications when compared to conventional RT.

1. Introduction

As radiation treatments continue to develop, new technologies aim to maximize the dose delivered to the treatment volume while minimizing the dose to the surrounding normal tissue. This is achieved by using the dose escalation method and improving radiation delivery systems. Implementation of image guided radiation therapy is now a key component for accurate patient set-up based on imaging systems. Daily cone-beam CT scans are performed to accurately set up patients in preparation of delivering the prescribed dose to the tumor. Margins must be added to the tumor to ensure a proper treatment volume dose coverage. The added margin may result in increased irradiation of healthy tissue and, consequently, higher normal tissue complications.[1] There has been great interest to investigate the implementation of magnetic resonance imaging (MRI) during radiation therapy. The MR guided radiotherapy improves the accuracy of such treatments due to improved soft tissue delineation and the capability of real-time tumor tracking.[2,3] The impact of this technique in radiation therapy has been evaluated by several investigators. Many researchers have investigated the effect of a magnetic field on electron and photon dose distributions.[4–8] Some investigators have evaluated the added challenges of magnetic fields for commonly irradiated geometries in radiotherapy when treating early-stage non-small cell lung cancer.[9,10] It has been documented that for these systems dose perturbations may occur in the patient due to the Lorentz force and the electron-return effects (EREs).[11] Currently, some standalone commercial treatment planning algorithms are used to model dose for MR-linac RT.[12] The treatment planning optimization can improve the dose distributions over the planning target volume (PTV) and the surrounding normal tissue to compensate for dosimetric perturbations caused by the presence of a strong magnetic field. Some manufacturers have started combining MRI and linear

* Corresponding author.
E-mail addresses: s-gholami@sina.tums.ac.ir (S. Gholami), franzlongo1969@gmail.com (F. Longo), Sarash@gmail.com (S. Shahzadeh), Nedaieha@sina.tums.ac.ir (H.A. Nedaie), rsharp156@gmail.com (R. Sharp), Alimeig@gmail.com (A. S.Meigooni).

https://doi.org/10.1016/j.rpor.2020.09.002
1507-1367/

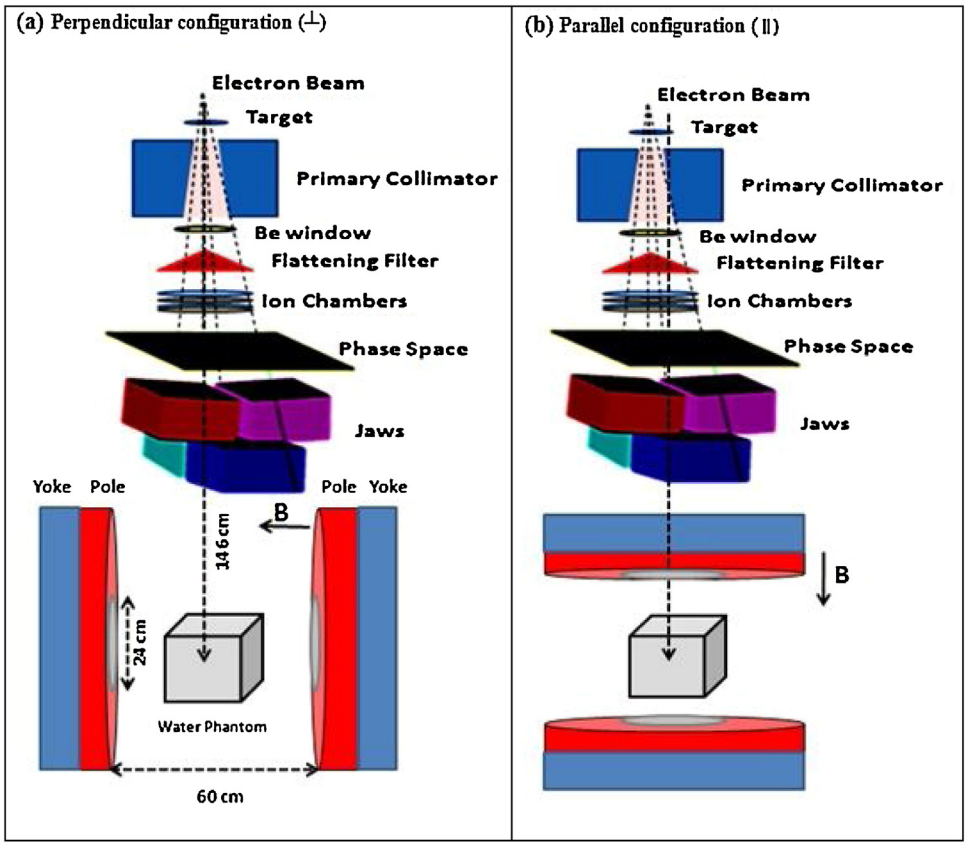

Fig. 1. Schematic configuration of the simulated linac head for both (a) perpendicular and (b) parallel magnetic field configurations.

accelerator systems into one system, allowing a real-time visualization of truly adaptive radiation therapy.[13]

MR-linac and conventional RT techniques differ with respect to their definition of clinical target volume (CTV) to PTV margin.[14] This results in different dose distributions for the NLT. It is desired to determine the complications in NLT based on its calculated dose volume histogram obtained from the RT techniques mentioned above.

The goal of the present study is to evaluate the impact of MR-linac RT on reducing the complications to the NLT. Monte Carlo (MC) simulation methods and the Niemierko NTCP model[15] have been used in these investigations. In these evaluations, three key parameters that correlate to the complications of the surrounding normal tissue receiving radiation are MLD, V_{20}, and NTCP. These parameters are used to compare patients treated with MR-linac against those treated with conventional RT.

2. Materials and methods

2.1. Monte Carlo simulation

Geant4 (version 10.1.p02) was applied for all simulations in this project. This toolkit is useful for simulating particles traversing through matter.[16]

The EmLivermorePhysics C++ class was used in the program to consider electron and photon interactions with material.[17] In Geant4, the threshold for tracking electrons and photons is defined as a distance or an energy cut-off range.[18] A 1 mm range cut-off was selected which corresponds to an energy cut-off of 5 keV for photons, and 350 keV for electrons. This cut-off range is well covered by a low energy package for electromagnetic interactions.[19] The differential equation solver, Classical Runge–Kutta, in Geant4 was used for calculating the trajectory of charged particles in a magnetic field.[16]

2.2. Linear accelerators

A model of the Varian clinical linear accelerator (Clinac 2100, Varian Medical Systems, Palo Alto, California, USA) head was simulated according to detailed geometry from the vendor. Simulations were performed in two steps. First, a new scored plane was created as a phase space file at the end of the treatment head of the Clinac. Then, the phase space file acted as a source for simulating the dose distribution in the water phantom/digital phantom. For the MR-linac configuration, we have used the same setup as Keyvanloo et al. study.[20] According to this study, the treatment assemblies were positioned along the beam axis such that the distance from the linac target to the isocenter was 146 cm. Fig. 1 shows the schematics of simulated geometries for both perpendicular (⊥) and parallel (||) configurations. The magnet assembly consists of a yoke structure made of carbon steel material and a pair of magnetic pole pieces made of magnetic steel.[20,21] The properties of the yoke material keep the magnetic field intensity at low magnetization, while the magnetic steel provides higher values of magnetization.[22] In MR-linacs the magnetic pole pieces act to enhance the magnetic field strength and improve the field homogeneity in the imaging volume.[23] According to Keyvanloo's et al.[20] study, the pole-to-pole separation was considered to be 60 cm with a 24 cm hole diameter of the bore through the yoke and pole structures. The simulated water phantom has dimensions of $16 \times 16 \times 16$ cm^3 which were divided into a set of voxels with dimensions of $2 \times 2 \times 2$ mm^3 and located at the isocenter.

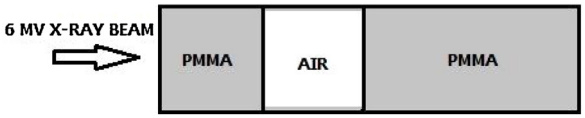

Fig. 2. Simulated geometry based on Raaijmakers et al's study[25] in order to test the magnetic field effect accuracy on relative depth dose by Geant4 MC toolkit.

2.3. Monte Carlo simulation validation

Dose calculation accuracies regarding small radiation field sizes using Geant4 have been demonstrated in our previous study.[24] We applied a 1.3 T magnetic field in MC calculations in order to test the accuracy of the simulated dose distributions in the presence of a magnetic field and compared our results to Raaijmakers et al. measured data.[25] In their study, dose distributions in the presence of a 1.3 T perpendicular magnetic field were measured for a 6 MV x-ray beam. We used similar phantom geometry which was composed of a 4-cm-thick air gap surrounded by a 4 cm and 8 cm thick PMMA phantom (Fig. 2).

In the rest of the study, a 1.5 T magnetic field was selected in the Geant4 simulation in order to investigate NLT complications. This selection has been based on some clinical reports which used this strength.[26–28] One simulation was performed in the presence of a 1.5 T magnetic field, perpendicular to the direction of the photon beam, and another simulation was performed without a magnetic field. The lung chemical composition data used in this study was taken from publications from the National Institute of Standard and Technology.[29] The lung, soft tissue/tumor, and bone densities were 0.3, 1.0 and 1.5 g/cm^3, respectively.[30]

2.4. The 4D extended cardiac-torso (4D-XCAT) digital phantom

The 4D-XCAT digital phantom was used as a model to provide CT images of a patient with respiratory motion. Application of this phantom in creating CT images for radiotherapy use has been shown previously.[31]

In this study, 5 frames per respiration cycle were generated by the XCAT phantom. It is possible to insert different lesions into the created CT images from the phantom.[32] Spherical lesions with diameters of 3 and 4 cm were created and located in the lower and

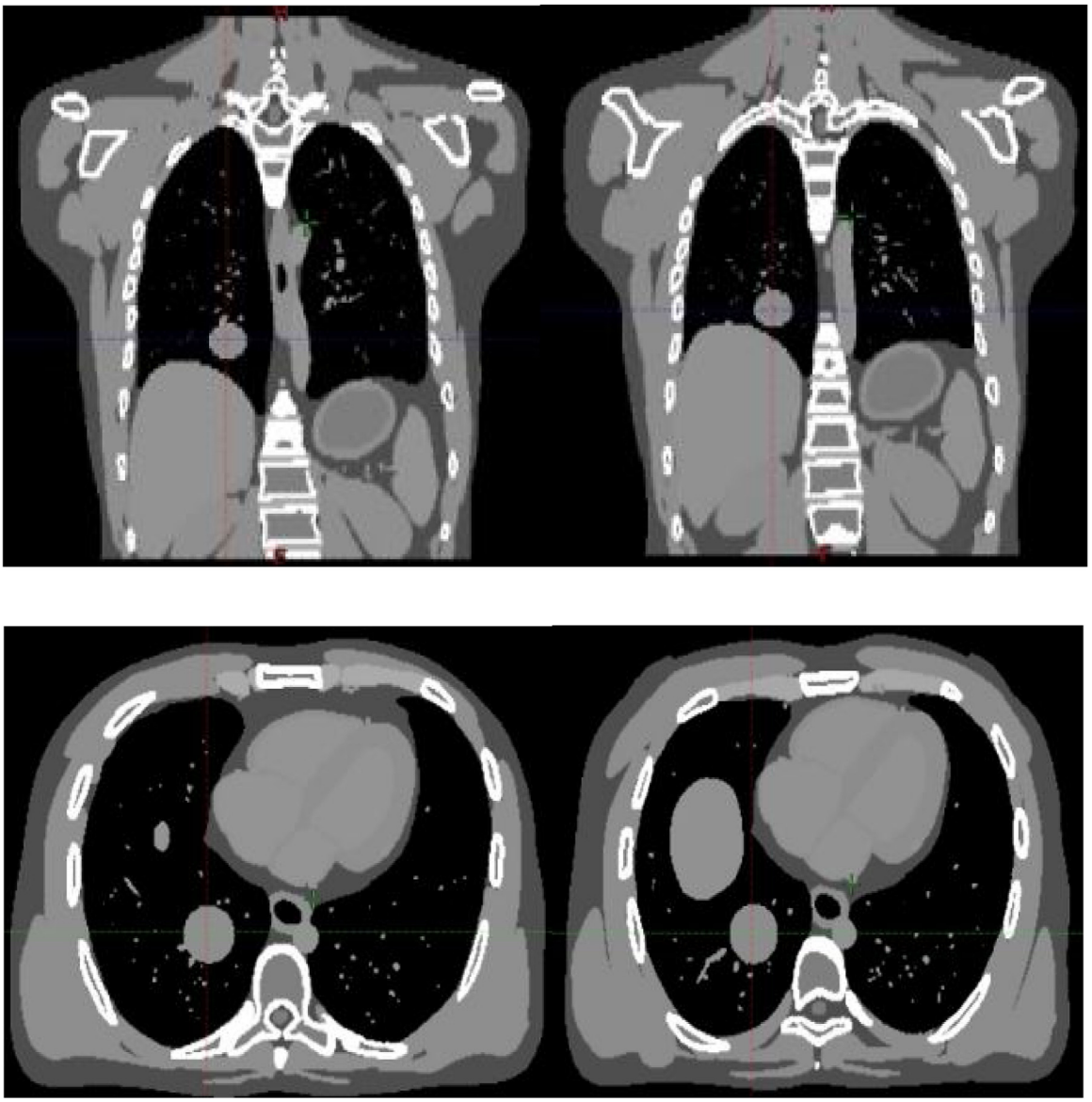

Fig. 3. 4D-CT images in 2 different respiratory phases generated by XCAT phantom.

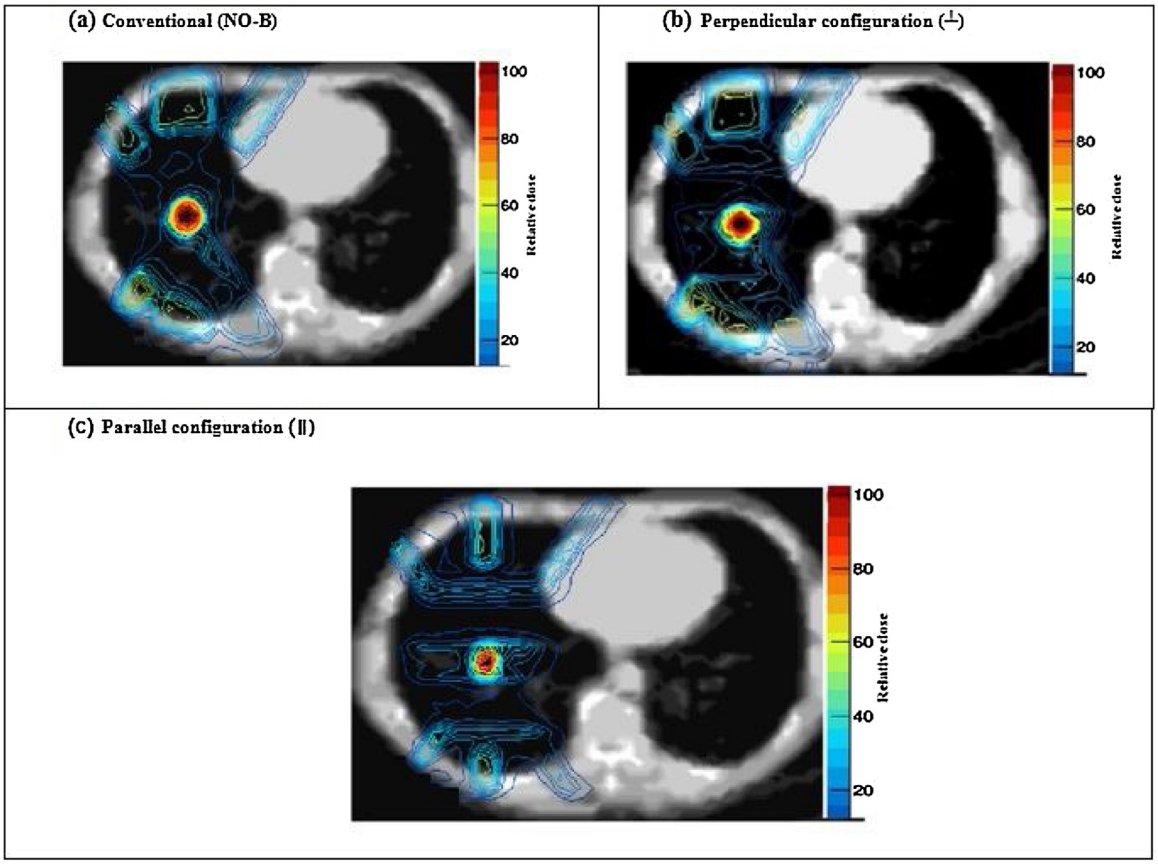

Fig. 4. An axial view of a converted DICOM image to the voxelized geometry in Geant4 and the dose distributions for the simulated lung tumor, calculated in Geant4 Monte Carlo engine for conventional (a) and MR-linac for the perpendicular (b) and parallel (c) configurations.

upper lobes of the phantom's lungs. A combination of the lesion and the digital phantom with the respiratory movements was utilized to represent movable tumors inside the lung.

The CTV was defined as the volume of the inserted lesions. In addition, for simulation of all images from the digital phantom, a diaphragm excursion of 2 cm was considered in input data of the phantom.

Fig. 3 shows the simulated 5-phase CT images which included a tumor located in the lower lobe of the right lung that is based on the XCAT phantom (breathing period: 5 s). MATLAB (7.8.0 Math Works, Natick, MA) software was used to convert the attenuation values (cm^{-1}) from the phantom to CT number (Hounsfield unit) and finally save it as a DICOM format.[33]

Using methods that have been previously established,[24] the CT DICOM files were converted to the Geant4 voxelized geometry format.[34] Further analysis included developing the program in Geant4 toolkit to use CT data for each hit position (in X,Y,Z voxels), using a sensitive detector method. The sensitive detector class in Geant4 has the task of creating hits (deposits of energy) each time a track traverses a sensitive volume and loses some energy.[16]

Tabulated data in the International Commission on Radiation Units and measurements (ICRU) report # 46 were used to convert Hounsfield unit values of each CT voxel to mass density and effective atomic number.[35]

2.5. MC-based engine for the dose calculations

Geant4 MC-based engine was used to calculate the relative dose distributions in the simulated patient with lung cancer for both MR-linac and conventional configurations. Due to the respiratory cycle,

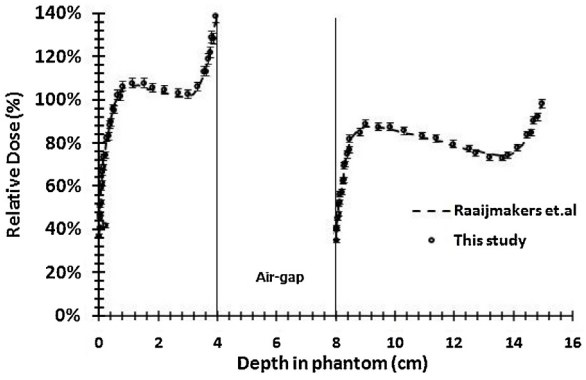

Fig. 5. Comparative graphs of central axis relative dose between this study (with 2% Error bars) and Raaijmakers's study in the presence of the magnetic field.

the motion of the CTV defines the internal target volume (ITV) for each target in accordance with ICRU Report 62.[36]

Two different margin approaches were used for each configuration to define the PTV. For conventional RT, standard PTV margins expanded the ITV by 8 mm isotropically. Meanwhile, for the MR-linac technique, a smaller PTV using reduced margins of approximately 3 mm was suggested.[14] The dose distributions for the simulated lung tumor were calculated in the Geant4 engine for conventional RT and for a MR-linac.

Fig. 4 shows an axial view of a DICOM image converted to the voxelized geometry in Geant4 for conventional (no-B) and MR-linac for the perpendicular and parallel configurations. For all treatment plans, the prescribed doses were 60 Gy using 6 independent conformal beams. A simple forward method was applied to optimize

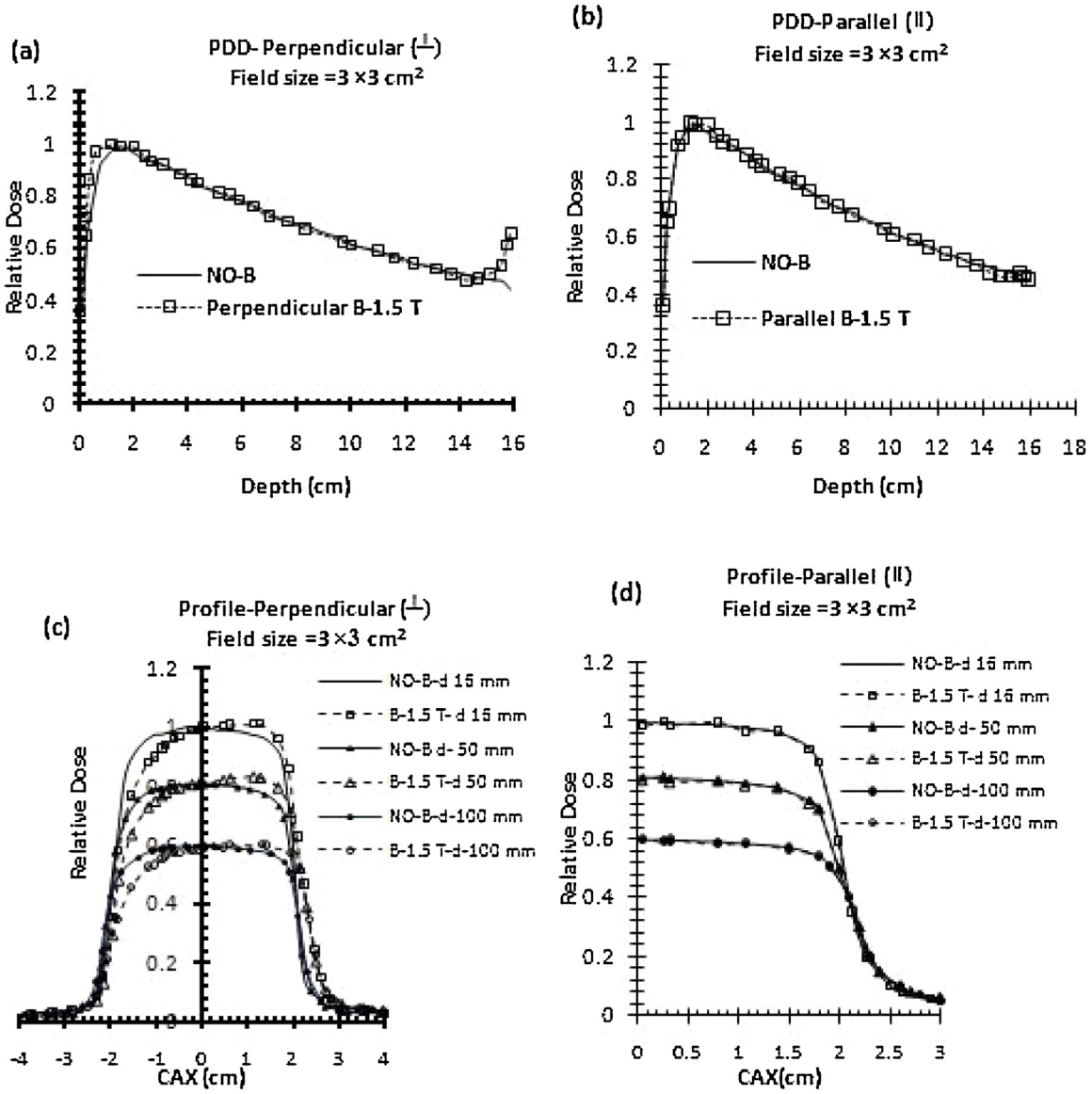

Fig. 6. Effect of magnetic fields on PDD curves and cross plane profile curves for perpendicular (a,c) and parallel (b,d) configurations for the field size of 3 × 3 cm^2.

relative beam weighting of each radiation beam to compensate for dosimetric perturbations caused by the presence of a strong magnetic field and cover the tumor with the 95% isodose line. For simplicity, the multi-leaf collimators have not been considered in the planning in order to reduce the computational time.

2.6. Normal lung tissue complication

The MLD,[37] V_{20},[38] and NTCP of the lung were calculated to anticipate pneumonitis as a complication of NLT for each RT method.

A MATLAB script was developed to compute the NTCP values for each method according to the formulism that was initially introduced by Niemierko15. The model is well defined in the AAPM report No.166.[39]

The differential dose volume histogram was directly exported from the MC engine and used in the NTCP calculation program. Then, the dose values were converted into the biological equivalent physical dose (EQD2) using equation (2).[40,41]

$$EQD_2 = D^* \frac{(\frac{\alpha}{\beta} + \frac{D}{n_f})}{(\frac{\alpha}{\beta} + 2)} \quad (2)$$

In the above Equation, D and n_f are the total prescribed dose and number of fractions, respectively. α and β are the tissue-specific parameters in the radiobiological linear-quadratic model. The *EUD* is calculated according to inhomogeneous dose distribution of each volume, $v_{i,}$ receiving the dose EQD_i. [40]

$$EUD = \left[\sum_{i=1}^{N} v_i \cdot \{EQD_i\}^a\right]^{\frac{1}{a}} \quad (3)$$

Where a is a unit-less model parameter that is specific to the normal structure of interest. Finally, the NTCP of the organ is calculated according to Equation 4.[15,42]

$$NTCP = \frac{1}{1 + \left[\frac{TD_{50}}{EUD}\right]^{4\gamma_{50}}} \quad (4)$$

γ_{50} is the slope of a dose response curve of normal tissue at 50% complication probability.[40]

$$\gamma_{50} = TD_{50} \cdot \frac{dNTCP}{dD}\Big|_{D=TD_{50}} \quad (5)$$

Table 1
For both MR-linac and conventional plans (a) Mean lung doses (MLDs) as a function of lesion diameter and its location (b) V_{20} for the normal lung tissue as a function of tumor size and its location (c) The calculated EUDs as a function of tumor sizes and its location (the diaphragm excursion is 20 mm.).

(a)						
MLD (Gy)						
Lesion location	Lesion diameter = 3cm			Lesion diameter = 4cm		
	MR-linac (∥)	MR-linac(⊥)	Conventional	MR-linac(∥)	MR-linac(⊥)	Conventional
RLL	12.0	14.4	17.0	16.6	18.0	21.3
LLL	10.1	12.1	14.2	14.8	16.1	19.0
RUL	6.5	7.4	8.6	8.9	9.8	10.7
LUL	9.0	10.0	11.4	12.0	13.2	14.4
(b)						
V_{20} (%)						
LesionLocation	Lesion diameter = 3cm			Lesion diameter = 4cm		
	MR-linac (∥)	MR-linac(⊥)	Conventional	MR-linac (∥)	MR-linac(⊥)	Conventional
RLL	26.3	27.9	36.9	32.7	33.3	46.3
LLL	19.5	21.0	27.3	27.5	29.4	36.1
RUL	11.2	12.7	14.5	14.2	15.6	17.6
LUL	15.7	17.4	20.4	19.0	20.5	23.0
	(c)					
	EUD (Gy)					
LesionLocation	Lesion diameter = 3cm			Lesion diameter = 4cm		
	MR-linac (∥)	MR-linac(⊥)	Conventional	MR-linac (∥)	MR-linac(⊥)	Conventional
RLL	11.0	12.4	15.1	15.5	16.8	20.0
LLL	9.3	10.5	12.6	14.2	15.0	18.0
RUL	6.1	7.6	8.2	8.4	9.0	9.7
LUL	8.2	9.8	10.7	9.9	10.5	11.6

Table 2
NTCPs of the lung for MR-linac (⊥ &∥) and conventional RT.

CASE	MR-linac RT(∥) NTCP(%)	MR-linac RT(⊥)	Conventional RT
RLL (T.S = 3 cm, diaph = 20 mm)	0.19%	0.28%	1.84%
RLL (T.S = 4 cm, diaph = 20 mm)	4.72%	7.20%	16.42%
LLL (T.S = 3 cm, diaph = 20 mm)	0.03%	0.05%	0.50%
LLL (T.S = 4 cm, diaph = 20 mm)	0.89%	1.90%	7.90%
RLL (T.S = 3 cm, diaph = 25 mm)	0.33%	1.79%	2.95%
RLL (T.S = 4 cm, diaph = 25 mm)	6.30%	8.40%	18.10%
LLL (T.S = 3 cm, diaph = 25 mm)	0.13%	1.10%	1.53%
LLL (T.S = 4 cm, diaph = 25 mm)	0.94%	1.05%	8.65%
RLL (T.S = 3 cm, diaph = 30 mm)	0.85%	1.65%	4.62%
RLL (T.S = 4 cm, diaph = 30 mm)	8.87%	10.17%	23.68%
LLL (T.S = 3 cm, diaph = 30 mm)	0.15%	0.71%	2.94%
LLL (T.S = 4 cm, diaph = 30 mm)	1.32%	2.40%	9.09%
RUL,LUL (T.S = 3&4 cm, diaph = 20–30 mm)	Less than 1%	Less than 1%	Less than 1%

RLL: Right Lower Lobe; LLL: Left Lower Lobe; T.S: Tumor size; diaph: the diaphragm excursion.RUL: Right Upper Lobe; LUL: Left Upper Lobe.

According to Eq. 4, for the endpoint of pneumonitis for normal lung tissue, "50% complication probability (TD50)"," γ_{50}" , "α/β" and "a" parameters were considered to be equal to 24.5 Gy; 2, 3 and 1, respectively.[15,43,44]

3. Results

3.1. Magnetic field simulation validation

Validation of the magnetic field calculations in our simulation showed that dose is increased by nearly 39%, when compared to the non-magnetic field case in the PMMA- air interface. Ahmad et al.[12] also reported a 40% higher deposited dose at the water-lung interface for a 1.5 T magnetic field. The difference in the results of these two magnetic field strengths (1.3 and 1.5 T) is considered negligible.

In Fig. 5, the calculated dose distributions along the central axis in the presence of the perpendicular magnetic field are in agreement within 2%/2 mm for more than 90% of the points as compared to the data reported by Raaijmakers et al.[25]

Fig. 6 (a,b) shows the relative depth dose (PDD) in the absence and presence of a 1.5 T magnetic field for perpendicular and parallel MR-linac configurations. For a perpendicular configuration, there is more than a 20% difference at the distal end of the PDD curve in comparison to the applied magnetic field and non-magnetic field. In addition, the maximum dose points in the buildup region are shifted to shallow depths.

Fig. 6 (c,d) shows the relative cross plane profiles at three different depths in the absence and presence of a 1.5 T magnetic field of perpendicular and parallel MR-linac configurations for a field size of 3×3 cm^2. In the parallel configuration, the profiles remain unchanged. The profiles have been shifted to the left side for per-

pendicular configuration due to the imposed force of magnetic field on secondary electrons.

3.2. MLD, V_{20}, EUD and NTCP for MR-linac and conventional RT

Tables 1 (a), (b), and (c) present a comparison between the tumor size, its location, MLDs, V20 s, and EUDs for both MR-linac and conventional radiation therapy techniques, respectively.

Furthermore, MLD, V_{20}, and EUD were lower for MR-linac RT, especially for the parallel configuration. The largest reduction of MLD, V_{20}, and EUD with MR-linac RT were 5 Gy, 29.3% and 4.1 Gy, respectively.

Table 2 shows that lung NTCPs are lower in the MR-linac ($\perp$ &$\parallel$) RT in comparison with the conventional RT. Here, too, this reduction is higher for parallel configuration (up to 15%) and the tumors that were in the lower lobe of the lung and near the diaphragm.

For the tumors located in the upper lobes, where the tumor motion was small, NTCP values of the lung were insignificant in both RT techniques (< 1%).

4. Discussion

In the first part of this study we simulated the MR-Linac irradiation in the presence of a 1.3 T magnetic field in order to validate the accuracy of the simulation in an inhomogeneous phantom and compared it to the published measured data.[25] Then a 1.5 T magnetic field was applied in MC simulation in both parallel and perpendicular directions. We have considered this strength due to some clinical reports in this strength. Ahmed et al.[12] and Raaijmakers et al.[25] reported around a 40% higher deposited dose at the water-lung interface for a 1.5 T and 1.3 T magnetic field. The difference in the results of these two magnetic field strengths (1.3 and 1.5 T) seems negligible. Finally, calculated NTCP values in MR-Linac and conventional radiotherapy were compared with each other.

The results from PDD profiles show that in the perpendicular geometry, the dose profiles shift asymmetrically away from the beam axis at all depths in the presence of the magnetic field. A similar study has shown the effect on the dose profile as reported by Raaymakers et al.[45] They show that the dose deposition changes asymmetrically in the direction perpendicular to the magnetic field which is seen in our profiles as well. For PDD curves, there are two differences: one in the buildup region and the other at the distal part of the PDD curve. Depth of the maximum dose was found shallower (~3–4 mm) in the presence of a magnetic field. The reason is that electrons travel curved pathways and deposit their energy at relatively shorter distances from the surface in a magnetic field. The increase of relative dose at the distal part of the PDD curve is due to ERE. Such an effect on dose profiles have also been reported by Ahmad et al.[12] and Raaijmakers et al.[25] In the parallel geometry the beam profiles (and penumbras) do not change as compared to non-magnetic field case for all depths, which is in agreement with Kirkby et al., using the EGSnrc simulation code.[28]

Due to EREs an increase in the dose was found to occur at the distal end of lung tissue. However, the increase of this dose is insignificant when considering the negligible effect it has on the clinically relevant parameters, such as EUD, V20, MLD, and NTCP values. The increase of dose may be due to the EREs at the air tissue interfaces, such as the chest wall and lung or the mediastinum and lung.

The reduction in lung NTCP in the MR-linac technique is due to reducing the CTV-to-PTV margin rather than more uniform dose distributions and, as the results showed, the magnetic field tends to make some hot and cold sub regions to the irradiated volume. However, in general, it can be said that using the MR-linac configuration is reasonable and can reduce NLT complications.

5. Conclusion

In this study, we investigated the benefits of MR-linac RT versus conventional RT in a simulation study. Despite the disturbance in dose distributions (cold and hot points) in the presence of the magnetic field, the MR-linac RT can lead to lower complications in NLT compared to the conventional RT.

Financial support

This research has been supported by Tehran University of Medical Sciences and Health Services with grant number 97-01-207-38000.

Conflict of interest

The authors declare that they have no conflict of interest.

Acknowledgments

This research has been supported by Tehran University of Medical Sciences and Health Services with grant number 97-01-207-38000.

References

1. Kilburn JM, Lucas JT, Soike MH, et al. Is a Clinical target volume (CTV) necessary in the treatment of lung cancer in the modern era combining 4-D imaging and image-guided radiotherapy (IGRT)? *Cureus*. 2016;8(1).
2. Menten MJ, Fast MF, Nill S, Kamerling CP, McDonald F, Oelfke U. Lung stereotactic body radiotherapy with an MR-linac–Quantifying the impact of the magnetic field and real-time tumor tracking. *Radiother Oncol*. 2016;119(3):461–466.
3. Ramey SJ, Padgett KR, Lamichhane N, et al. Dosimetric analysis of stereotactic body radiation therapy for pancreatic cancer using MR-guided Tri-60Co unit, MR-guided LINAC, and conventional LINAC-based plans. *Pract Radiat Oncol*. 2018.
4. Bielajew AF. The effect of strong longitudinal magnetic fields on dose deposition from electron and photon beams. *Med Phys*. 1993;20(4):1171–1179.
5. Earl M, Ma L. Depth dose enhancement of electron beams subject to external uniform longitudinal magnetic fields: A Monte Carlo study. *Med Phys*. 2002;29(4):484–491.
6. Chen Y, Bielajew AF, Litzenberg DW, Moran JM, Becchetti FD. Magnetic confinement of electron and photon radiotherapy dose: A Monte Carlo simulation with a nonuniform longitudinal magnetic field. *Med Phys*. 2005;32(12):3810–3818.
7. Jette D. Magnetic fields with photon beams: Dose calculation using electron multiple-scattering theory. *Med Phys*. 2000;27(8):1705–1716.
8. Shao W, Tang X, Bai Y, et al. Investigation of the dose perturbation effect for therapeutic beams with the presence of a 1.5 T transverse magnetic field in magnetic resonance imaging-guided radiotherapy. *J Cancer Res Ther*. 2018;14(1):184.
9. Kirkby C, Murray B, Rathee S, Fallone B. Lung dosimetry in a linac-MRI radiotherapy unit with a longitudinal magnetic field. *Med Phys*. 2010;37(9):4722–4732.
10. Park JM, Park S-Y, Kim HJ, Wu H-G, Carlson J, J-i Kim. A comparative planning study for lung SABR between tri-Co-60 magnetic resonance image guided radiation therapy system and volumetric modulated arc therapy. *Radiother Oncol*. 2016;120(2):279–285.
11. St Aubin J, Keyvanloo A, Vassiliev O, Fallone B. A deterministic solution of the first order linear Boltzmann transport equation in the presence of external magnetic fields. *Med Phys*. 2015;42(2):780–793.
12. Ahmad SB, Sarfehnia A, Paudel MR, et al. Evaluation of a commercial MRI linac based monte carlo dose calculation algorithm with geant 4. *Med Phys*. 2016;43(2):894–907.
13. Foley A, Hybrid Linac-MR. Image-guided radiation therapy delivered in real-time. *Microw J (Int Ed)*. 2013;56(12):54.
14. Bainbridge HE, Menten MJ, Fast MF, Nill S, Oelfke U, McDonald F. Treating locally advanced lung cancer with a 1.5 T MR-Linac–Effects of the magnetic field and irradiation geometry on conventionally fractionated and isotoxic dose-escalated radiotherapy. *Radiother Oncol*. 2017;125(2):280–285.
15. Gay HA, Niemierko A. A free program for calculating EUD-based NTCP and TCP in external beam radiotherapy. *Phys Med*. 2007;23(3-4):115–125.
16. Agostinelli S, Allison J, Amako KA, et al. GEANT4—A simulation toolkit. *Nucl Instrum Methods Phys Res A*. 2003;506(3):250–303.
17. Ivanchenko V, Apostolakis J, Bagulya A. Recent improvements in Geant4 electromagnetic physics models and interfaces. *Prog Nucl Sci Technol*. 2011;2:898–903.
18. Collaboration G. Geant4 User's Guide for Application Developers. Accessible from the GEANT4 web page [1] Version Geant4. 2012;9.

19. Grevillot L, Frisson T, Maneval D, Zahra N, Badel J, Sarrut D. Simulation of a 6 MV Elekta Precise Linac photon beam using GATE/GEANT4. *Phys Med Biol*. 2011;56(4):903.
20. Keyvanloo A, Burke B, Warkentin B, et al. Skin dose in longitudinal and transverse linac-MRIs using Monte Carlo and realistic 3D MRI field models. *Med Phys*. 2012;39(10):6509–6521.
21. Tadic T, Fallone BG. Three-dimensional nonaxisymmetric pole piece shape optimization for biplanar permanent-magnet MRI systems. *IEEE Trans Magn*. 2011;47(1):231–238.
22. Gloria N, Areiza M, Miranda I, Rebello J. Development of a magnetic sensor for detection and sizing of internal pipeline corrosion defects. *NDT & e International*. 2009;42(8):669–677.
23. Tadic T, Fallone BG. Design and optimization of a novel bored biplanar permanent-magnet assembly for hybrid magnetic resonance imaging systems. *IEEE Trans Magn*. 2010;46(12):4052–4058.
24. Gholami S, Longo F, Nedaie HA, Berti A, Mousavi M, Meigooni AS. Application of Geant4 Monte Carlo simulation in dose calculations for small radiosurgical fields. *Med Dosim*. 2017.
25. Raaijmakers A, Raaymakers BW, Lagendijk JJ. Experimental verification of magnetic field dose effects for the MRI-accelerator. *Phys Med Biol*. 2007;52(14):4283.
26. Raaymakers B, Jürgenliemk-Schulz I, Bol G, et al. First patients treated with a 1.5 T MRI-Linac: Clinical proof of concept of a high-precision, high-field MRI guided radiotherapy treatment. *Phys Med Biol*. 2017;62(23):L41.
27. Fast M, van de Schoot A, van de Lindt T, Carbaat C, van der Heide U, Sonke J-J. Tumor trailing for liver SBRT on the MR-linac. *Int J Radiat Oncol Biol Phys*. 2019;103(2):468–478.
28. Kirkby C, Stanescu T, Rathee S, Carlone M, Murray B, Fallone B. Patient dosimetry for hybrid MRI-radiotherapy systems. *Med Phys*. 2008;35(3):1019–1027.
29. https://www.nist.gov/pml/productsservices/physical-reference-data. 2017; https://www.nist.gov/pml/productsservices/physical-reference-data.
30. Berger MJ, Hubbell JH, Seltzer SM, Coursey JS, Zucker DS. *XCOM: Photon cross section database (version 1.2). http://physics. nist. gov/xcom*; 1999.
31. Panta RK, Segars P, Yin F-F, Cai J. Establishing a framework to implement 4D XCAT phantom for 4D radiotherapy research. *J Cancer Res Ther*. 2012;8(4):565.
32. Mishra P, James Ss, Segars Wp, Berbeco Ri, Lewis Jh. Adaptation and applications of a realistic digital phantom based on patient lung tumor trajectories. *Phys Med Biol*. 2012;57(11):3597.
33. Dunn L. *Assessing the impact of motion on treatment planning during stereotactic body radiotherapy of lung cancer*; 2013.
34. Kimura A, Aso T, Yoshida H, Kanematsu N, Tanaka S, Sasaki T. *DICOM data handling for Geant4-based medical physics application. Paper presented at: Nuclear science symposium conference record*. 2004 IEEE; 2004.
35. White G, Wilson I. Photon, electron, proton and neutron interaction data for body tissues. *ICRU Report*. 1992;46.
36. Wambersie A, Landgerg T. ICRU report 62: Prescribing, recording and reporting photon beam therapy. *ICRU Publ Bethesda MD*. 1999.
37. Wang W, Xu Y, Schipper M, et al. Effect of normal lung definition on lung dosimetry and lung toxicity prediction in radiation therapy treatment planning. *Int J Radiat Oncol Biol Phys*. 2013;86(5):956–963.
38. Videtic GM, Hu C, Singh AK, et al. A randomized phase 2 study comparing 2 stereotactic body radiation therapy schedules for medically inoperable patients with stage I peripheral non-small cell lung cancer: NRG Oncology RTOG 0915 (NCCTG N0927). *Int J Radiat Oncol Biol Phys*. 2015;93(4):757–764.
39. Li XA, Alber M, Deasy JO, et al. The use and QA of biologically related models for treatment planning: Short report of the TG-166 of the therapy physics committee of the AAPM. *Med Phys*. 2012;39(3):1386–1409.
40. Oinam AS, Singh L, Shukla A, Ghoshal S, Kapoor R, Sharma SC. Dose volume histogram analysis and comparison of different radiobiological models using in-house developed software. *J Med Phys*. 2011;36(4):220.
41. Voyant C, Julian D, Roustit R, Biffi K, Lantieri C. Biological effects and equivalent doses in radiotherapy: A software solution. *Rep Pract Oncol Radiother*. 2014;19(1):47–55.
42. Surega A, Punitha J, Sajitha S, Ramesh B, Pichandi A, Sasikala P. A statistical quantification of radiobiological metrics in Intensity Modulated Radiation Therapy evaluation. *Gulf J Oncolog*. 2015;1(17):15–23.
43. Newcomb C, Van Dyk J, Hill R. Evaluation of isoeffect formulae for predicting radiation-induced lung damage. *Radiother Oncol*. 1993;26(1):51–63.
44. Shahzadeh S, Gholami S, Aghamiri SMR, Mahani H, Nabavi M, Kalantari F. Evaluation of normal lung tissue complication probability in gated and conventional radiotherapy using the 4D XCAT digital phantom. *Comput Biol Med*. 2018;97:21–29.
45. Raaymakers B, Lagendijk J, Overweg J, et al. Integrating a 1.5 T MRI scanner with a 6 MV accelerator: Proof of concept. *Phys Med Biol*. 2009;54(12):N229.